Studying the Detectability of High Mass Black Hole Binary Mergers with Future Gravitational Wave Detectors

LIGO SURF 2021 Final Paper September 24, 2021

Author: Sabrina Barbaro[1]
Mentors: Alan Weinstein[2]*, Richard Udall*[2]

[1]Boston University, U.S.
[2]California Institute of Technology, U.S.
sbarbaro@bu.edu, ajw@caltech.edu, rudall@caltech.edu

Abstract

In this work we determined the distances to which gravitational waves from Intermediate Mass Black Hole Binary (IMBHB) mergers can be detected by ground based gravitational wave detector network in observing run four (O4), and beyond. Binary black hole mergers between 65 and 150 $M_{\odot}$ are predicted to be rare as a result of pair instability in the final stages of their progenitor stars, so future observations of IMBHB mergers will help us to understand formation processes. Therefore this study seeks to calculate the detectability of IMBHB mergers for future runs of the detector network. We determine the sensitive luminosity distance of merger events within the IMBH mass range, averaged over other astrophysical parameters. Optimal sensitivity distances are given for several detector network configurations, including predictions for future detectors. Additionally we present detection efficiency predictions as a function of redshift, and distance horizon value for various high mass mergers. We present the sensitive volume of the detector network, and predict the number of IMBHB merger events we expect to observe in future runs.

Index Terms: distance horizon, intermediate mass black holes, pair pulsational instability, binary black holes, black hole binary mergers, waveform models, gravitational waves.

1. Introduction

1.1. Overview of the Study

Black holes (BHs) can be found throughout the universe in binary pairs which orbit each other. Energy is lost in these orbital systems, in the form of gravitational waves (GWs) as time goes on until these binary black holes (BBHs) become close enough to merge together as a type of compact binary coalescence (CBC). This project aims to determine the luminosity distances to which gravitational waves from Intermediate Mass Black Hole Binary (IMBHB) [1] mergers can be detected in observing run four (O4), and beyond, of the Gravitational Wave Detector network (GWDN). By using waveform approximant models, like the IMRPhenom model family, to simulate gravitational wave strain (in either the time or frequency domain) produced from the merger of binary black holes (BBHs) we will study the factors that affect sensitivity; specifically those in the intermediate mass range. Considering these simulated strains —averaged over several physical attributes of the merger and external parameters specific to observation —will allow the prediction of the distance sensitivity to be expected for future observing runs.

These simulations use predetermined ratios of fifteen astrophysical parameters [2], that will be sampled over to create a random population. Since IMBHB mergers are expected to be very rare, occurring at a rate density of $0.13^{+0.30}_{-0.11}\ Gpc^{-3}yr^{-1}$, based on the single event GW190521 [1], determining the future sensitivity distance relates directly to increased chance of detecting them, since an increase in sensitive distance correspond to cubic increase in space-time volume (VT). These VTs refer to the co-moving spacetime volume, which experiences cosmological redshift of the GW signal (time domain waveforms/frequency/BBH mass) and time dilation. Strictly speaking this makes the relationship between distance and volume less than cubic. Additional considerations during waveform correction will include detector antenna response from the gravitational wave detector network. The corrected waveforms will be categorized as detectable or not by the network of detectors based on the SNR values calculated for them. Ultimately this will determine the sensitive distance to which GWs from IMBHB mergers will be detectable in upcoming observing runs.

1.2. Gravitational Wave Background

Binary black holes, predicted and later confirmed with the detection of GW150914 [2], are thought to arise from co-evolved binary star systems or dynamical capture in dense stellar environments [3]. Once formed general relativity (GR) predicts that the black holes (BHs) will orbit each other, losing energy in the form of gravitational radiation and move closer together, until finally merging into a single object [4]. The gravitational waves produced by BBH mergers are a result of the relativistic orbit that ripples space-time [5], emitted at a frequency equivalent to twice of the orbital frequency [6]. Gravitational wave data are consistent with GR so far, so waveform simulations used throughout this study are based on GR simulations.

Although GWs are produced by all moving matter in the universe, only merging events of neutron stars and black holes are loud enough to be visible to the current gravitational wave

[1]Explained in depth in section 2.3, Motivation, for the purposes of this study we will refer to black holes between 50 and 250 $M_{\odot}$ as intermediate mass, and systems as IMBHBs if at least one of the constituent black holes falls within this range. This is in order to consider black holes in the pair instability/pulsational pair instability mass gap.

[2]The fifteen parameters include the individual BBH masses, the three spin components for each BH, orientation of the orbitals plane (with respect to the line of sight), azimuthal angle, luminosity distance, time of coalescence, phase of coalescence, right ascension and declination. We will assume circular orbits.

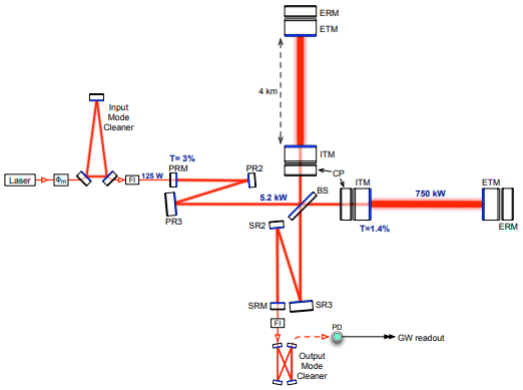

Figure 1: *Advanced LIGO schematics [[11], fig.2]*

detector network. In gravitational wave physics terminology, "loud" refers to a GW signal that has a large strain amplitude in the detector's sensitive frequency band, resulting in a high signal-to-noise ratio (SNR). Even still, not all mergers are visible to the network; the 3rd LIGO Virgo run (O3, from April 2019 through March 2020) effectively required an SNR of around 12 or more [7] for an event to be distinguishable from noise in the data. Additionally the recorded data had to be within the GWDN frequency band, between 20 Hz to 2048 Hz [8], to be detected. We take these basic conditions to dictate what can be detected by the GWDN for the purposes of this study, despite the more nuanced detection criteria on real data. We explore the multiple intrinsic and external variables that can affect whether the strain data collected from a merger will meet this preliminary criteria.

The gravitational wave detector network uses Michelson Interferometers to measure the GWs, in which the mirrors of the detector are freely suspended and the interferometer bounces lasers down each mirror arm. A passing GW will stretch and compress the arm cavities and create a phase difference between the lasers used to sense the separation between the mirrors, quantified as strain of the 4 km-long detector arms (or 3 km, for Virgo) [9]. The gravitational waves arriving at the detectors are measured from their distortion of space in this manner, which is collected as strain data characterized by the following relation [10]:

$$h = h_+ F_+ + h_\times F_\times. \tag{1}$$

Where h is the strain, plus and cross represent the polarizations, and F represents the detector antenna response to each polarization. Each polarization's strain is dependent on the intrinsic properties of the merger event, whereas the detector antenna response is dependent on the detector's antenna response to varying sky location and orbital orientation with respect to the detector.

This strain, h, is seen by the gravitational wave detector network only if it both is above the SNR detection threshold and within the GWDN frequency band. The SNR of a merger event can be calculated with the matched filter SNR formula [12]:

$$\langle a|b\rangle = 4\int_{f_{low}}^{f_{high}} \frac{\tilde{a}(f)\tilde{b}^*(f)}{S_n(f)} e^{2\pi i f t} df. \tag{2}$$

To find the optimal SNR the template, a, must exactly matche the signal b, and $t = 0$, such that [13]:

$$\langle a(\theta,f)|b(\theta,f)\rangle = 2\int_{f_{low}}^{f_{high}} \frac{a(\theta,f)b(\theta,f)^* + c.c}{S_n(f)} df \tag{3}$$

Where $a(\theta, f)$ is the strain in the frequency domain, $b(\theta, f)$ is the (GR-based) gravitational waveform template that best fits the data (maximizing the SNR), and $S_n(f)$ is the power spectral density of the detector noise. This optimal SNR relationship is also applicable to simulated strains, which will enable predictions of the BBH mergers visible in observation run 4 and beyond.

1.3. Astrophysical Motivation for Finding Distance Sensitivity of High Mass Binaries

Astrophysicists predict a deficit of black holes whose progenitor stars are between the masses of about 95 $M_\odot$ and 130 $M_\odot$ [13] attributed to the pulsational pair instability mass gap. Stars that begin hydrogen fusion at this mass may undergo a pulsational pair instability supernova near the ends of their lives due to the internal thermal conditions. Stars outside of this mass range, conversely, may transition to their final states more immediately, be they black holes, neutron stars, white dwarfs, or others. The stars in the pair instability mass range finish their hydrogen fusion and begin to form heavier cores, containing helium and other heavy elements up until the typical iron (and nickel) barrier for stellar fusion. The pressure, and thermal energy, within these heavy cores will build through each burning stage until the heat reaches a critical temperature, exceeding $10^9 K$ [13], at which point the environment creates electron-positron pairs from photons. While the photons provided thermal pressure to support the star's radius, the pair instability electrons and positrons contribute significantly less outward pressure, which leads to disruption of the star's hydro-static equilibrium. The electron-positron pairs are created with a cascading effect, so large quantities of thermal energy go into creating these particle pairs which do little to support the stars radius, eventually leading to overall contraction of the star due to lack of pressure. A chain effect soon follows; the sudden contraction, and therefore increased temperature, creates a period of explosive element burning, providing more fusion pressure within the star, which in turn causes an increase in radius that may be fast enough and ejects many solar masses worth of material from the star. Pair instability stars may be completely decimated from this collapse, but pulsational pair instability stars may go through this cycle many times over, losing layers of mass each time. After the ejection the pulsational stars will contract again, releasing both light and neutrinos, and encounter another instability; a process that repeats until it reaches a stable mass around 65 $M_\odot$, with a heavy core of 40 $M_\odot$ [13]. The succeeding pulses will eject less material, but have higher energy, and can collide with the initial material becoming extremely luminous [13].

Due to the Pulsational Pair Instability (PPI) and Pair Instability (PI) processes there is a predicted gap in the black hole mass spectrum, roughly in the range from 50 - 135 $M_\odot$ range [14]; but the boundaries of this range are rather uncertain. However with the discovery of GW190521, a high mass BBH merger, during observing run 3 of the LIGO and Virgo detector network, researchers were able to confirm one of the constituent black holes was in the IMBH range. The GWs originated from a BBH merger with constituent masses of 66 $M_\odot$ and 85 $M_\odot$, leaving behind a remnant of 142 $M_\odot$ [1]. There are contending theories on the production of IMBHs such as this, like hierarchical merging of many smaller black holes [15], or primordial

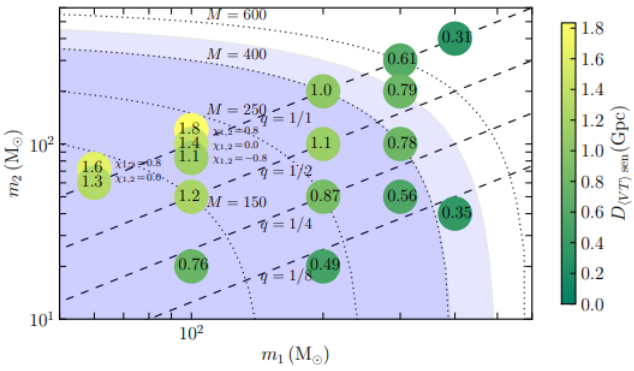

Figure 2: *Distance sensitivity, in Gpc, of IMBHB merger events with varying constituent masses [[17], fig.1].*

origins allowing for masses in this range [16].

Since the formation mechanisms for the GW190521 and other IMBHB mergers are currently unknown, there is hope that the method by which IMBHB systems form could help clue in how super massive black holes form. Thus detecting more IMBHB mergers is crucial for developing our understanding, yet these events are few and far between with such a low production rate of $0.13 Gpc^{-3} yr^{-1}$ [1]. This project aims to estimate the sensitive volume and event rate for detection of GWs from BBH mergers containing high mass black holes, with data from current and future ground-based detector networks.

Determining the distance sensitivity of the detector network has been important in past observing runs as well. In observing runs one and two (O1 and O2) the sensitivity distance was calculated for differing constituent masses of IMBHB mergers, as shown below [17]. The maximum distance calculated by this previous study is around 1.8 Gpc [17] for optimal conditions of a 100 on 100 $M_\odot$ black hole, aligned-spin source. This project expects to see improved sensitivity distances due to better detector sensitivity in run 4, O4, and more advanced modeling.

2. Methodology

2.1. Gravitational Wave Simulation Tools

To calculate future sensitive volume this project uses simulated BBH merger waveforms using PyCBC waveform model families [18]. These models contain a wide variety of waveform templates, created by combining post-newtonian approximations of the early inspiral with numerical relativity solutions for the merger and ring-down portions of the event. These methods are used to reduce the computer time needed to produce the templates; post-newtonian approximations are faster than numerical relativity, and a variety of numerical techniques are employed to reduce the run time of general relativity simulations from a few months, typical of Spectral Einstein Code, to a few seconds [19]. The PyCBC waveform package takes advantage of these methods, giving us access to a wide variety of templates under varying parameters, without increasing uncertainty. The errors in the waveform families are comparable to the numerical errors in the original numerical relativity simulations. [19].

A decision between the waveform models offered by PyCBC must be considered for their potential impact on this study. After comparing several waveform model families we have determined the latest models are sufficiently similar for their differences to be negligible for the purposes of this study. We have chosen to utilize the IMRPhenomXP model to simulate waveforms. The IMRPhenom waveform family excels at simulating the early inspiral, which other families sometimes neglect to model. Due to the specific focus on distance sensitivity, longer waveforms may be helpful in recovering the most SNR during match filtering. Additionally the IMRPhenom waveform IMRPhenomXP is chosen over it's aligned spin counterpart, IMRPhenomXAS, in order to consider the individual spins of the component BHs.

We are interested in how precession of the orbital plane affects the detectability of a merger. When each component BH has spin aligned with the orbital angular momentum of the binary system, as modeled by IMRPhenomXAS, the system experiences a non-precessing orbit. However to model individual non-aligned component BH spins the waveform model must also take into account the precession of the system, like IMRPhenomXPHM. The IMRPhenomXPHM also takes into account the presence of higher order modes in the signal waveform, which is also of interest for affect on detectability.

2.2. Averaged Parameters and Sampled Parameters for Waveform Production

This study aims to provide average sensitivity estimates to IMBHB mergers over the whole sky, necessitating averaging over two main variable groups. In order to average we provide random values for each parameter and produce an array of samples to gauge the overall sensitivity. First, all sky location and orientation of the orbital plane with respect to the detectors variables are averaged to provide the overall sensitivity. The antenna patterns of the detectors are accounted for before averaging, but the final sensitivity prediction is not location specific. Second, the presence of non-aligned spin of the component black holes means we will consider two cases: binaries with component spins aligned with the orbital angular momentum, and binaries with randomly-oriented component spins. Considering both cases is needed in order to quantify how significant the effect of precessing spin is on the detectability and sensitive volume.

Conversely we sample over other variables to observe their effect on sensitivity to each detector network. We calculate the sensitivity as a function of component mass and redshift, which calls for even sampling of these two parameters. The combination of methods for choosing variables provides an overall sensitivity.

Figure 3 is an illustrative example waveform of a 25 on 75 $M_\odot$ merger at 3000 Mpc (a waveform that exists within our defined sample set), and the strain that would be detected by LIGO Livingston, LIGO Hanford, and Virgo. This is one of the waveforms that will be included in the averaging process in these particular mass and redshift bins[3]. The features of this waveform that are important to note includes the spin-induced amplitude modulation, and the difference in observed strain in each detector.

Figure 4 is the corresponding frequency domain data for the same simulated signal, in comparison to the LIGO Livingston noise amplitude spectral density (ASD). The small oscillations from 30-50Hz are a visible result of the same amplitude modulation seen in the time domain graph. This particular merger event falls well within the GWDN band, spending more time at

[3] All waveforms are produced under the assumption of the flat lambda-CDM model when accounting for cosmological effects.

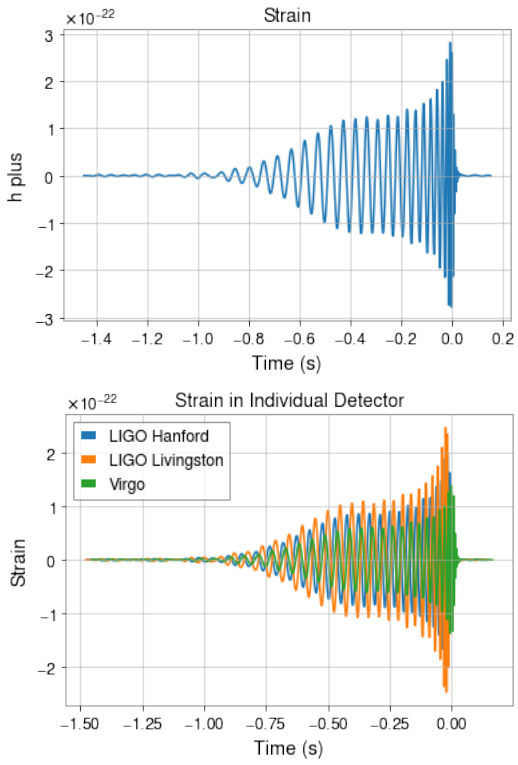

Figure 3: *An example of a simulated GW signal from a BBH merger event using random parameter selection. The waveform was produced with the IMRPhenomXP waveform approximant from PyCBC for two black holes of 75 $M_\odot$ and 25 $M_\odot$ at 3000Mpc. A slight spin-induced amplitude modulation is visible due to non-aligned component spins. The top graph is the strain of the GW plus polarization. The bottom graph is the strain each detector in the network would detect based on the binary's sky position.*

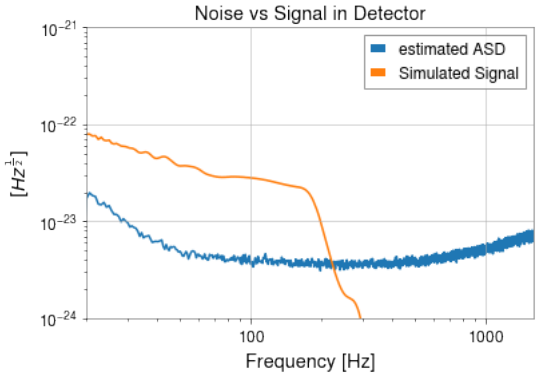

Figure 4: *The above is the frequency domain data corresponding to the event from figure 3. The blue line represents the estimated amplitude spectral density of the Gaussian noise in the detector, while the orange line is that of the magnitude of the signal, $|\tilde{b}(\theta, f)|$.*

lower frequencies, and we predict would be visible to the the network.

Additionally the amplitude tapering before the time of merger of the signal should be mentioned as non-representative of a real signal. A waveform from a BBH extends for millions of years into the past, however they are only typically modeled at frequencies above 20Hz because detector noise below this threshold overwhelms any signal. In order to avoid Gibb's noise when Fourier transforming the waveform models we taper strain under the lower frequency bound rather than having a sharp cut-off. The goal of averaging over these parameters is to eliminate dependencies on everything but the mass and distance of the merger event in the final sensitivity measurement.

2.3. Assumed Initial Conditions

In order to produce predictions for future observing runs, we must use assumptions for what future conditions will look like. Our calculations for O3 utilizes real data, in particular the real noise power spectral density (PSD), to determine the SNR of any given event. However we can not know the noise PSDs for the future, and therefore rely on the the idealized detector PSDs made available in the PyCBC software package [18]. These are most likely overly-optimistic, and will lead to slightly higher SNR values than would be realistically expected. In particular the low frequencies are expected to have higher noise than the PSDs we use in this study, so we may expect unrealistically high sensitivity to both high mass and high redshift systems.

In order to calculate the optimal SNR this study employs the matched filter SNR formula, equation two, while using a generated waveform for $\tilde{a}(\theta, f)$ and an exactly matching template for $\tilde{b}^*(\theta, f)$. The exact match of the waveform and the template gives the maximum SNR, however detector noise will reduce the SNR in real observed signals.

As we produce simulated data and predicted SNR, we must consider the metric for which we claim detection in comparison with search pipelines. In this work we threshold on the network SNR (sum of the individual detector SNRs in quadrature, since the noise is uncorrelated between detectors) such that if a given event has SNR above 12, we say it is detected by the detector network. In reality search pipelines use a combination of variables, along with SNR, to tag a candidate event. The use of idealized data and noise estimates we assume the methods typically used by search pipelines are unnecessary to evaluate detectability for the purposes of this study. Additionally we consider waveforms with both spin distributions and higher order modes (HOMs), factors which search pipelines do not include in their template banks. This work does address spin and HOMs in order to determine what effect they would have on detection ability.

When producing the number of IMBHB mergers expected to be observed in the future we must also consider the assumption that the detector network will will be in constant observing mode, with 100% duty cycle, and therefore observe all events. This is not a realistic expectation for future observing periods, so once again it should be expected that actual detections will be less than the value presented here.

2.4. Detector Frame

Once the source frame signal has been produced we must consider the varying detector antenna response. Detector response (Eqn (1)) is the reason for the discrepancy in strain, and time delay, seen in the bottom panel of figure 3. This example waveform would be most favorably oriented with respect to the LIGO-Livingston detector, based on the random sky location parameters given. At different sky locations the largest ampli-

tude could be from a different detector, which is why to determine the overall sensitivity this study will average over random sky locations and orientations.

In addition to detector sensitivity at any given sky location, the waveforms must be redshifted. This affects the amplitude, and frequency, of the strain detected, and will affect SNR and estimated parameters. The GWDN can record frequencies from 20 Hz up to 2048 Hz [8], at a SNR of about 12 [7]. A distant merger emitting waves can be redshifted outside of the GWDN band for higher mass systems, or into the band for very low mass systems. The masses inferred from the source frequency follow the relationship $M_{detector-frame} = M_{source-frame}(1+z)$, and the signal waveform $a(\theta, f)$ is evaluated at the redshifted mass, $M_{detector-frame}$. After taking into account the source frequency produced by the merger through redshifting the masses, this study determines how the following conditions affect a mergers final detectability: The amplitude of the signal is inversely proportional to the luminosity distance to Earth ($amplitude = \frac{1}{d_L}$), so some signals may be diminished below the detectable SNR, presumably not triggering a search pipeline. The presence/absence of precession and higher order modes affecting the resolution of the signal. Additionally the orientation of the event being favorably located in relation to the detector network (optimal location and orientation events are directly over a detector and face-on) [20] will influence the individual detector's chances of finding a signal in the background noise. After these final considerations we can use the detection efficiencies to determine the expected sensitive volume for each scenario.

In order to make predictions for future sensitivity we must use assumptions for which detectors will be operational, and process data under these hypothetical configurations. For this purpose we will consider four different GWDN configurations as follows: O3 (where O3 is the only configuration using actual PSDs) consisted of LIGO-Hanford, LIGO-Livingston, and Virgo; O4 will consist of LIGO-Hanford, LIGO-Livingston, Virgo, and KAGRA; O5 will consist of LIGO-Hanford, LIGO-Livingston, Virgo, KAGRA, and LIGO-India; and CE will consist of LIGO-Hanford, LIGO-Livingston, Virgo, KAGRA, LIGO-India, and Cosmic Explorer [4]. As a note the detectors that are currently operational use their present PSDs for future predictions.

3. Results

In this section we present several measurements of sensitivity to IMBHB mergers as functions of; total system mass in solar masses, the q mass ratio of the constituent black holes ($q = \frac{m_2}{m_1} \leq 1$), and distance in terms of redshift and luminosity distance under a flat lambda-CDM model assumptions of the Astropy [21] Planck15 cosmology. Under this cosmology the value for $H_0 = 67.7$ and $\Omega_m = 0.307$. These results require further study as there are some blatant issues with the results presented in this section. In the tables and the figures it is clear that the estimates for IMBHB merger sensitivity are far too low. There is also an absence of a predicted sensitivity increase, of several factors, between O3 and future observing runs.

3.1. Effective Distance Sensitivity for Varied Parameters

Here the effective sensitivity distance predictions are given based on BBH merger system properties. Firstly, the most important fact is that the efficiency of detection for IMBHB mergers falls off as a function of distance. The fall off is dictated both by distance, and system parameters, thus we may consider efficiency as: $\epsilon(z|\theta)$, for some redshift, z, and parameter combination, θ. In this section we examine how varying parameters effects the function ϵ, and give key examples of the differences.

The first factors we examine are the total mass, and mass ratios of the system. We consider mass ratios between $\frac{1}{6}$ and 1, of the smaller BH compared to the larger BH. In figure 5 we have included efficiency curves under varying mass combinations to illustrate these differences. In sub-figure (a) the shape of the efficiency curve behaves as expected for a signal moving out of detection range. On the other hand, in sub-figures (b) and (c) cosmological effects influence the shape of the curve and the concavity of the curves as they approach zero efficiency. Here the shape indicates that the detection efficiency experiences a sharper cut-off due to the system frequencies being redshifted out of the GWDN frequency band. Here the strain in the detectors would be strong enough to be feasibly identified above the noise if the detectors were sensitive to the lower frequencies of these signals. In sub-figure (d) the efficiency curve has a shape very similar to (a), however the differentiating feature is the range of luminosity distances spent at 100% efficiency, up until 300 Mpc. Sub-figure (d) uses the predicted O5 network configuration, including LIGO-Hanford, LIGO-Livingston, LIGO-India, Virgo, and KAGRA, which will have significantly more sensitivity than the O3 configuration. Therefore we predict to have essentially 100% detection efficiency for these distances relatively close to Earth.

The 100% detection efficiency region, as seen in figure 5(d), leads to an important note on the CE configuration. Cosmic Explorer, which is included in the CE network, is expected to have extremely high detection sensitivity. Using the sensitivity estimates for Cosmic Explorer we expect to have some events be completely at 100% efficiency within the distance range considered in this study, or in other words, some flat efficiency curves. Additionally the frequency range of Cosmic Explorer should increase to include down to 5Hz [22], which means that signals with high mass, or at high redshifts, will remain within the detectable range.

An alternate way of visualizing distance sensitivity as a function of the mass parameters is shown in figure 6. Here the predicted distance for which 50% of events will be detected is given at different mass ratios of the constituent BHs. Increasing distance sensitivity with increased mass is expected, where the slow decrease in sensitivity at higher masses is due to cosmological redshift out of the GWDN frequency band. Overall sensitivity distance is seen to increase with q, up until q=1; meaning that systems with very unbalanced BH masses produce far fainter strain than those with similar masses. Although there is some tipping point such that slightly unequal masses produce marginally higher strain than perfectly equal masses.

Finally the distance sensitivity can be observed comparatively to determine which factors included in this study have the most significant effects on detectability. Table 1 provides some key qualitative examples of how parameters including masses, precession, and presence of higher order modes, affects maxi-

[4] The Cosmic Explorer configuration is likely actually consist of 2 to 3 detectors similar to Cosmic Explorer at different locations. For the purposes of this study however, the 6 detectors listed above will be used.

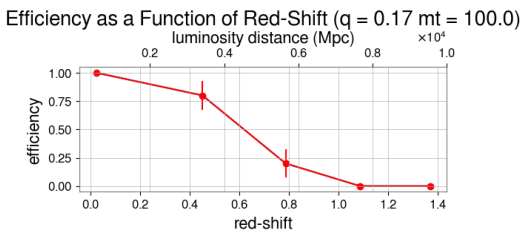

(a) *Network O3*

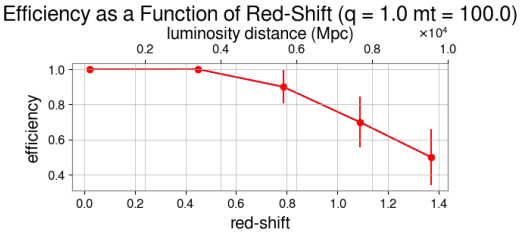

(b) *Network O3*

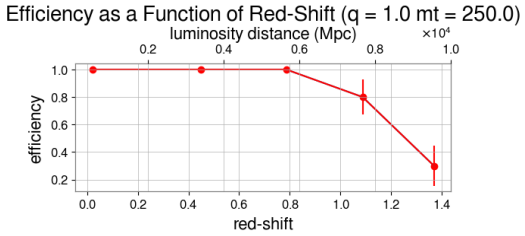

(c) *Network O3*

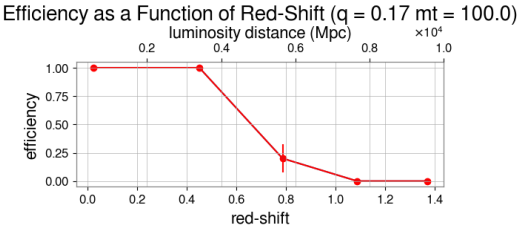

(d) *Network O5*

Figure 5: *Detection efficiency functions of IMBHB merger systems as functions of redshift. These plots illustrate the effects that intrinsic mass parameters, and increased network sensitivity in plot d, have on efficiency. The effects of frequency band redshifting are visible in plots b, c, and d.*

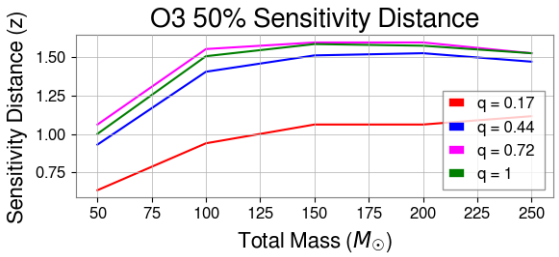

Figure 6: *50% Sensitivity distance, as redshift, for BBH mergers. The lines represent mass ratios of the total system mass, from $\frac{1}{6}$ to 1.*

Maximum Distance Sensitivity by redshift Parameter, z		
Parameters	Total Mass/ Mass Ratio	Distance
Net = O3, no precession/HOMs	M_t = 50, q = 0.17	0.6347
Net = CE, no precession/HOMs	M_t = 50, q = 0.17	1.649
Net = O3, no precession/HOMs	M_t = 150, q = 1.0	1.584
Net = O3, precession/HOMs	M_t = 150, q = 1.0	1.584
Net = O3, no precession/HOMs	M_t = 250, q = 1.0	1.525
Net = CE, no precession/HOMs	M_t = 250, q = 1.0	1.649

Table 1: *Demonstrated above is the sensitivity affect additional detectors are predicted to have on maximum distance sensitivity, and the small impact of precession/higher order modes on detectability. Additionally in the last two rows we notably fail to observe a comparatively large increase in distance sensitivity due to the redshift experienced by high mass systems being ultimately shifted out of the GWDN band of sensitivity.*

mum sensitivity distance. In particular the third and fourth row of the table examine the effect of precesssion and HOMs on detectabilty, highlighting the fact that there is little to no change due to their presence, even in IMBHB systems.

3.2. Predicted Number of Events for Network Configurations

Here we present estimates for how many events will be observed by each detector configuration for IMBHB mergers in the 65-250 $M_\odot$ mass range. The following formula was used to determine the number of events to be detected based on the possible efficiency of detection:

$$N = RT \int \epsilon(z|\theta) \frac{dV_c}{dz} \frac{1}{(1+z)} \cdot dz \tag{4}$$

where

R is the event rate per $Gpc^{-3}yr^{-1}$

$\frac{T}{(1+z)}$ is time with a cosmological correction factor

z is redshift factor

ϵ is the efficiency function from section 3.1

θ are parameters of the merger system

$\frac{dV_c}{dz}$ is the differential co-moving volume.

Given this definition the predicted number of events observed per year with each detector configuration is given in table 2. The rate used in this calculation is the $0.13^{+0.30}_{-0.11}\ Gpc^{-3}yr^{-1}$ [1] as measured from GW190521 by the LIGO Scientific Collaboration and Virgo Collaboration. The rate is expected to be related to distance and the formation methods of IMBHBs, which is unfortunately unknown. We therefore unrealistically approximate the rate R to be independent of redshift / cosmological evolution for this calculation.

The results presented in Figures 5 and 6, and Tables 1 and 2, are not in accord with our expectations. Most notably, we expect future detector networks to yield much larger numbers of detected IMBHB events than is reported in Table 2. It is likely that, in addition to low statistics (low numbers of simulations),

Network	Predicted Number of Events
O3	0.178
O4	0.189
O5	0.189
CE	0.290

Table 2: *Estimates of how many IMBHB merger events will be observed by the GWDN according to various detector configurations. These estimates are made under the conditions described in Section 2, Methodology. To also be considered is that the detectors are taken to be in constant observing mode.*

there are bugs in the code used to produce them; more debugging is required.

4. Conclusion

In this work we evaluated the effects of astrophysical and detector based factors on the detection capabilities of IMBHB mergers by the gravitational wave detector network. We established two different sensitivity metrics, namely sensitivity distance and number of expected events according to the detector network. In addition to network configuration, these calculations were performed considering precession and higher order modes factors, which current search pipelines do not account for.

The results presented in Section 3 represent a work in progress. They are too preliminary and uncertain to draw meaningful conclusions - that will require further study. They do, however, present the kinds of figures and numbers that can be used (after proper debugging) to draw conclusions about the effects of interest to us when estimating detected event counts: the dependence on mass, mass ratio, spins, precession, and higher order modes; and the effect of present and future detector networks with increasing sensitivity.

If, however, we take the results in Section 3 at face value, they show several important relationships that will have results on the detection efficiency for IMBHB mergers:

- Network configuration has the most significant impact on detectability, and rightfully so. More detectors, and more sensitive detectors, will increase the ability to identify all events; including IMBHB merger events. Since IMBHB mergers are not plentiful within our immediate region of space, we must consider large space-time volumes for their detection, which can correspond to low strain response in the GWDNs. Increased sensitivity will ensure that merger signals reaching Earth are more likely to be identified as event candidates.
- The amplitude of the GW signal is predominantly determined by the mass and mass ratio of the black holes in the system, which is directly tied to detection efficiency. In cases where mass redshifting is small/negligible there is a direct relationship between heavier systems and better detection sensitivity. However for the majority of systems in the IMBHB mass range redshift plays an important role, and can be expected to play a significant role in reducing the detection sensitivity for imminent observing runs.
- Both precession and the presence of higher order modes in the waveforms were examined for their possible impact on detectabilty of IMBHB systems. In this study the waveform with these effects is compared to a template including precession and HOM effects, yielding high SNRs. Search pipelines however do not include these features while identifying candidates, and may therefore miss merger events. In follow-up study the waveforms including these features can be compared to a template without them in order to determine the factor it diminishes SNR.

4.1. Future Work

The results of the study were somewhat limited by the mass ratio bounds of the PyCBC library. The values presented here are tentative and require validation in future work. In a follow-up study of detectability it would be informative to push the limits of the mass values considered, as well as the maximum redshifts of the signals. Additionally including the effects of more nuance in the calculations, like using the rate as a function of redshift $R(z)$, could increase the accuracy of the presented results. By comparing predicted event numbers to observed event numbers it is also possible to determine the best model for $R(z)$.

5. Acknowledgments

I thank Alan Weinstein and Richard Udall for their tremendous support in this project. I also gratefully acknowledge the support from the National Science Foundation Research Experience for Undergraduates (NSF REU) program (award 1852081), the California Institute of Technology, the LIGO Summer Undergraduate Research Fellowship, and the family of Carl Albert Rouse.

6. References

[1] LIGO Scientific Collaboration and Virgo Collaboration, *"GW190521: A Binary Black Hole Merger with a Total Mass of 150 $M_{\odot}$,"* Phys. Rev. Lett. 125, 101102 (2020), Sep 2020.

[2] LIGO Scientific Collaboration and Virgo Collaboration, *"Observation of Gravitational Waves from a Binary Black Hole Merger"* Phys. Rev. Lett. 116, 061102 (2016)

[3] The LIGO Scientific Collaboration, the Virgo Collaboration, *"Astrophysical Implications of the Binary Black-Hole Merger GW150914 ,"* ApJL, 818, L22, 10.3847/2041-8205/818/2/L22, 2016.

[4] LIGO Scientific Collaboration, *"Tests of General Relativity with Gravitational Waves from Black Hole Mergers,"* https://ligo.org/science/Publication-O2TGR/flyer.pdf.

[5] LIGO Scientific Collaboration, *"Background of Gravitational Waves Expected from Binary Black Hole Events Like GW150914,"* https://www.ligo.org/science/Publication-GW150914Stoch/index.php.

[6] Robert C. Hilborn, *"Gravitational waves without general relativity: A tutorial,"* Am. J. Phys. 86, 186-197 (2018), 10.1119/1.5020984.

[7] Abbott, B. P. et al., KAGRA Collaboration, LIGO Scientific Collaboration, and Virgo Collaboration, *"Prospects for observing and localizing gravitational-wave transients with Advanced LIGO, Advanced Virgo and KAGRA,"* 10.1007/s41114-020-00026-9, 2020.

[8] LIGO Scientific Collaboration and, Virgo Collaboration, *"GWTC-2: Compact Binary Coalescences Observed by LIGO and Virgo During the First Half of the Third Observing Run,"* Phys. Rev. X 11, 021053 (2021), 10.1103/PhysRevX.11.021053

[9] LIGO Scientific Collaboration *"Introduction to LIGO Gravitational Waves,"* https://www.ligo.org/science/GW-IFO.php

[10] John Whelan, *"Visualization of Antenna Pattern Factors via Projected Detector Tensors,"* LIGO Document T1100431-v2, 2012.

[11] LIGO Scientific Collaboration, *"Advanced LIGO,"* 10.1088/0264-9381/32/7/074001, 2014.

[12] LIGO Scientific Collaboration and Virgo Collaboration, *"GW150914: First results from the search for binary black hole coalescence with Advanced LIGO,"* Phys. Rev. D 93, 122003 (2016), 10.1103/PhysRevD.93.122003.

[13] Yiwen Huang, Carl-Johan Haster, Salvatore Vitale, Aaron Zimmerman, Javier Roulet, Tejaswi Venumadhav, Barak Zackay, Liang Dai, and Matias Zaldarriaga, *"Source properties of the lowest signal-to-noise-ratio binary black hole detections,"* 10.1103/PhysRevD.102.103024, LIGO P2000082, 2020.

[13] S. Woosley, S.Blinnikov, and A. Heger, *"Pulsational pair instability as an explanation for the most luminous supernovae,"* Nature 450, 390–392 (2007), https://doi.org/10.1038/nature06333.

[14] K. Belczynski, A. Heger, W. Gladysz, A. J. Ruiter, S. Woosley, G. Wiktorowicz, H.-Y. Chen, T. Bulik, R. O'Shaughnessy, D. E. Holz, C. L. Fryer, and E. Berti, *"The effect of pair-instability mass loss on black-hole mergers"* AA, vol. 594, A97, Oct 2016, https://doi.org/10.1051/0004-6361/201628980.

[15] B. McKernan, K. E. S. Ford, W. Lyra, and H. B. Perets, *"Intermediate mass black holes in AGN disks: I. Production Growth,"* Mon.Not.Roy.Astron.Soc.425.1:460–469,2012, 10.1111/j.1365-2966.2012.21486.x.

[16] T. Kawaguchi, M. Kawasaki, T. Takayama, M. Yamaguchi, J. Yokoyama *"Formation of intermediate-mass black holes as primordial black holes in the inflationary cosmology with running spectral index,"* Mon.Not.Roy.Astron.Soc.388:1426-1432,2008, 10.1111/j.1365-2966.2008.13523.x.

[17] LIGO Scientific Collaboration and Virgo Collaboration, *"Search for Intermediate Mass Black Hole Binaries in the First and Second Observing Runs of the Advanced LIGO and Virgo network,"* Phys. Rev.D 100, 064064 (2019), 10.1103/PhysRevD.100.064064.

[18] Nitz, A. H., Harry, I., Brown D., Biwer, C. M., et al., PyCBC Software, Zenodo, Version 1.16.14. Nov. 1 2021, URL: https://pycbc.org, doi:10.5281/zenodo.5347736

[19] J. Blackman, S. E. Field, C. R. Galley, B. Szilagyi, M. A. Scheel, M. Tiglio, D. A. Hemberger, *"Fast and accurate prediction of numerical relativity waveforms from binary black hole coalescences using surrogate models,"* Phys. Rev. Lett. 115, 121102 (2015), 10.1103/PhysRevLett.115.121102.

[20] Thesis Library Caltech, *"Introduction to LIGO,"* ch.3, https://thesis.library.caltech.edu/1901/9/08chap3.pdf.

[21] Astropy Collaboration, Astropy Software, Version 4.3.1., Nov. 1 2021, URL: https://astropy.org, doi: 10.1051/0004-6361/201322068

[22] Evan D. Hall, Kevin Kuns, Joshua R. Smith, Yuntao Bai, Christopher Wipf, Sebastien Biscans, Rana X Adhikari, Koji Arai, Stefan Ballmer, Lisa Barsotti, Yanbei Chen, Matthew Evans, Peter Fritschel, Jan Harms, Brittany Kamai, Jameson Graef Rollins, David Shoemaker, Bram Slagmolen, Rainer Weiss, Hiro Yamamoto, *"Gravitational-wave physics with Cosmic Explorer: limits to low-frequency sensitivity"* Phys. Rev. D 103, 122004 (2021), 10.1103/PhysRevD.103.122004